POLITECNICO DI TORINO
Repository ISTITUZIONALE

Topological Fitting: broadband modeling of passive components via augmented equivalent circuit models

(Article begins on next page)

25 April 2024

Topological Fitting: broadband modeling of passive components via augmented equivalent circuit models [★]

Sanda Lefteriu[*] Stefano Grivet-Talocia[**]

[*] IMT Lille Douai, France (e-mail: sanda.lefteriu@imt-lille-douai.fr).
[**] Politecnico di Torino, Italy (e-mail: stefano.grivet@polito.it)

Abstract: This paper presents a gray-box modeling technique for obtaining physical models of electrical components. These models are obtained through topological fitting, thus yielding equivalent electrical circuit models which are guaranteed to be stable and passive. The algorithm finds the values of the circuit elements given a description of the circuit such that the resulting model fits the frequency response measurements provided for the component. Moreover, in case the circuit is incomplete, the algorithm extends it by automatically generating all series and parallel augmentations and re-optimizing the values of the elements.

1. INTRODUCTION

The increase in the operating frequency of integrated circuits require broadband component models to be easily included in a simulator. Hence equivalent circuit models (ECMs) are designed to take into account parasitic, skin and proximity effects, which are present in high-frequency.

Broadband models are typically developed for each component using physical insight: spiral inductors (Cao et al. (2003); Wang et al. (2006)), ceramic capacitors (Sullivan et al. (2002)), thin-film resistors (Li and Wei (2015)), etc. For large circuits, the number of possible topologies increases dramatically. The choice of element types and values is another issue. Alternatively, frequency responses (Z-,Y- or S-parameters) are used to fit a rational model via black-box system identification techniques, followed by circuit synthesis (Zhaoqing (2015)), however synthesis using only passive elements is not trivial. Passivity is crucial in circuit simulation because a stable but non-passive network may become unstable for certain terminations.

This paper aims to make a step towards a fully-automated circuit generation for components described by frequency domain measurements. Oftentimes, one already has some preliminary idea of the topology of an incomplete ECM of a given component or subsystem (nominal circuit). This model can be enhanced by the addition of elements to improve its accuracy. We propose to generate all possible augmentations of the nominal circuit by inserting elements in series or in parallel to the existing ones. To find the optimal value of the added elements, we solve the resulting nonlinear optimization problem via a Sanathanan-Koerner iteration combined with an alternating least-squares.

Previous approaches for automated broadband model generation were not able to ensure stability and passivity by construction. In Kolstad et al. (2006), the error between the available measurements and the response of the nominal circuit is modeled by a small number of pole-zero elements, so the final model consists of the ECM together with the augmentation network described as pole-zero elements, which are found by black-box fitting. Stability of the augmentation can be enforced by pole-flipping, while passivity is enforced a-posteriori. Paul et al. (2009) solves the same nonlinear optimization problem as in Eq. (15) by expressing the unknown as a rational function and the coefficients of numerator and denominator polynomials are found via least squares. Stability can be enforced by constraining the coefficients to stay positive, while passivity is enforced via perturbation of the purely imaginary eigenvalues of the Hamiltonian matrix pencil (Grivet-Talocia and Gustavsen (2015)). In our approach, we optimize the value of each added circuit element independently in an alternating least-squares setting, thus guaranteeing stability and passivity of the final model.

The paper is structured as follows. Section 2 presents a short review of the modified nodal analysis used to represent electrical circuits. In Sect. 3, we propose to perform all possible series and parallel augmentations of the nominal circuit. Sect. 4 discusses the proposed approach for topological fitting. Lastly, Sect. 5 presents numerical examples validating our approach and Sect. 6 concludes the paper.

2. CIRCUIT MODELING VIA MODIFIED NODAL ANALYSIS (MNA) - SHORT REVIEW

MNA (Ho et al. (1975); Vlach and Singhal (1983)) is a powerful technique for automatically formulating (and solving) circuit equations. Multi-port circuits are typically given in terms of their impedance (Z-), admittance (Y-), or scattering (S-) formulation:

- for the **impedance** formulation, the circuit is current-controlled at all ports and the corresponding voltages are measured as outputs: $\mathbf{V} = \mathbf{ZI}$, where $\mathbf{V} = [v_1 \ldots v_p]^T$ and $\mathbf{I} = [i_1 \ldots i_p]^T$ are the vectors of port voltages and currents, respectively, with p, the

number of ports (we assume, for each port, one input and one output variable).

- for the **admittance** formulation, the circuit is voltage-controlled at all ports and the corresponding currents are measured as outputs: $\mathbf{I} = \mathbf{Y}\mathbf{V}$.
- for the **scattering** formulation, at each port, the input is the incident wave $a = \frac{v + R_0 i}{2\sqrt{R_0}}$ and the output is the reflected wave $b = \frac{v - R_0 i}{2\sqrt{R_0}}$, where R_0 is the port reference impedance (typically 50Ω).

Nodes are defined such that there exists a single element between two nodes. For the simple RLC circuit in Fig. 1, nodes have been indicated by circled numbers. Node 0 is the ground (reference for node voltages).
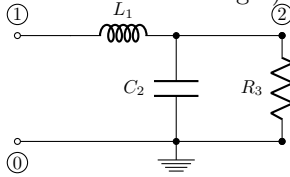

Fig. 1. RLC circuit

The topology of the circuit is described by the incidence matrix: the number of rows is the number of nodes in the circuit and each column corresponds to one branch which contains a single element. Each column is mostly zero, except for the rows given by the two nodes between which this element is connected, which contain 1 and -1. For the RLC circuit, the incidence matrix is:

$$\mathbf{A}_F = \begin{array}{c} ① \\ ② \\ ⓪ \end{array} \begin{matrix} 1 & 2 & 3 \\ \left[\begin{matrix} 1 & 0 & 0 \\ -1 & 1 & 1 \\ 0 & -1 & -1 \end{matrix}\right] \end{matrix}. \quad (1)$$

Kirchhoff's current law at each node yields the product between the incidence matrix and the branch currents being 0: $\mathbf{A}_F \mathbf{I}_b = \mathbf{0}$. The last equation is the negative of the sum of the previous ones, so we can disregard it and delete the last row to obtain the reduced incidence matrix:

$$\mathbf{A} = \begin{array}{c} ① \\ ② \end{array} \begin{matrix} 1 & 2 & 3 \\ \left[\begin{matrix} 1 & 0 & 0 \\ -1 & 1 & 1 \end{matrix}\right] \end{matrix}. \quad (2)$$

The Kirchhoff's voltage law expresses branch voltages $\mathbf{V}_b$ in terms of nodal voltages $\mathbf{E}$: $\mathbf{V}_b = \mathbf{A}^T \mathbf{E}$. KCL and KVL describe topological equations, which, together with the constitutive equations, yield the MNA formulation.

We distinguish between the following types of branches:

(1) shunt dynamic: a capacitor (branch 2),
(2) shunt resistive: a conductance (no such branch is present in our example),
(3) series dynamic: an inductance (branch 1)
(4) series resistive: a resistor (branch 3).

The columns of the incidence matrix are partitioned according to the type of element: shunt dynamic $i_C = [2]$, where i_C stores their indices, shunt resistive $i_G = [\ ]$, series dynamic $i_L = [1]$ and series resistive $i_R = [3]$:

$$\mathbf{A}_C = \begin{bmatrix} 0 \\ 1 \end{bmatrix}, \quad \mathbf{A}_G = [\ ], \quad \mathbf{A}_L = \begin{bmatrix} 1 \\ -1 \end{bmatrix}, \quad \mathbf{A}_R = \begin{bmatrix} 0 \\ 1 \end{bmatrix}. \quad (3)$$

We also define diagonal matrices storing the values of the elements depending on the type:

$$\mathbf{C}_b = [C_2], \quad \mathbf{G}_b = [\ ], \quad \mathbf{L}_b = [L_1], \quad \mathbf{R}_b = [R_3]. \quad (4)$$

For voltage controlled (shunt) elements, the constitutive equations are $\mathbf{i}_G = \mathbf{G}_b \mathbf{v}_G$ and $\mathbf{i}_C = s\mathbf{C}\mathbf{v}_C$, with s, the Laplace variable, while for current controlled (series) elements, they are $\mathbf{v}_R = \mathbf{R}_b \mathbf{i}_R$ and $\mathbf{v}_L = s\mathbf{L}_b \mathbf{i}_L$.

The unknowns of the MNA system are the node voltages and the branch currents for the series elements. These are included as state variables. In our case:

$$\mathbf{x}(t) = \begin{bmatrix} v_1 \\ v_2 \\ i_{L1} \end{bmatrix}.$$

The RLC circuit in Fig. 1 has one single port defined between nodes ① and ⓪, corresponding to one input and one output variable. We distinguish between the three formulations:

(1) impedance case: inputs are port currents and outputs are port voltages. Correspondingly, the input and output mapping matrices are

$$\mathbf{C} = [1\ 0\ 0\ 0], \quad \mathbf{B} = \mathbf{C}^T.$$

(2) admittance case: inputs are port voltages and outputs are port currents. Since the input current is not present in the vector of generalized state variables, we add a series resistive element (with zero-valued resistance), whose current will be our input variable. Correspondingly, the matrices after the update are:

$$\mathbf{A}_R = \begin{bmatrix} 0 & -1 \\ 1 & 0 \end{bmatrix}, \quad \mathbf{R}_b = \begin{bmatrix} R_3 & \\ & 0 \end{bmatrix}.$$

The input and output mapping matrices are

$$\mathbf{C} = [0\ 0\ 0\ 0\ 1], \quad \mathbf{B} = \mathbf{C}^T.$$

(3) scattering case: inputs are the incident waves and outputs are the reflected waves. Incident waves can be represented by series Thevenin sources with internal resistance R_0, hence the incidence matrix $\mathbf{A}_R$ should be updated with such new elements, and the diagonal $\mathbf{R}$ should be updated with a block containing the reference R_0 on the diagonal:

$$\mathbf{A}_R = \begin{bmatrix} 0 & -1 \\ 1 & 0 \end{bmatrix}, \quad \mathbf{R}_b = \begin{bmatrix} R_3 & \\ & R_0 \end{bmatrix}.$$

The input and output mapping matrices are

$$\mathbf{B} = \begin{bmatrix} 0 & 0 & 0 & 0 & 2\sqrt{R_0} \end{bmatrix},$$
$$\mathbf{C} = \begin{bmatrix} \frac{1}{2\sqrt{R_0}} & 0 & 0 & 0 & -\frac{\sqrt{R_0}}{2} \end{bmatrix}.$$

The descriptor matrices of the MNA formulation are

$$\mathbf{E}_{dae} = \begin{bmatrix} \mathbf{A}_C \mathbf{C}_b \mathbf{A}_C^T & \mathbf{0} & \mathbf{0} \\ \mathbf{0} & \mathbf{L}_b & \mathbf{0} \\ \mathbf{0} & \mathbf{0} & \mathbf{0} \end{bmatrix}, \ \mathbf{A}_{dae} = -\begin{bmatrix} \mathbf{A}_G \mathbf{G}_b \mathbf{A}_G^T & \mathbf{A}_L & \mathbf{A}_R \\ -\mathbf{A}_L^T & \mathbf{0} & \mathbf{0} \\ -\mathbf{A}_R^T & \mathbf{0} & \mathbf{R}_b \end{bmatrix} \quad (5)$$

and the transfer function is given by the usual formula

$$\mathbf{H}(s) = \mathbf{C}\left(s\mathbf{E}_{dae} - \mathbf{A}_{dae}\right)^{-1} \mathbf{B}, \quad (6)$$

which can represent the Z-,Y- or S-parameter formulation. $\mathbf{H}(s)$ is a rational matrix function of variable s and size p. This dynamical system is described by a differential algebraic equation with an invertible matrix pencil $(\mathbf{A}_{dae}, \mathbf{E}_{dae})$, a singular $\mathbf{E}_{dae}$ and the output equation having $\mathbf{D} = \mathbf{0}$:

$$\mathbf{E}_{dae}\dot{\mathbf{x}}(t) = \mathbf{A}_{dae}\mathbf{x}(t) + \mathbf{B}\mathbf{u}(t), \quad (7)$$
$$\mathbf{y}(t) = \mathbf{C}\mathbf{x}(t). \quad (8)$$

3. CIRCUIT AUGMENTATION

Given a nominal (starting) circuit, it is possible to insert elements in series or in parallel according to these rules:

(1) parallel augmentations with shunt elements between any two existing nodes if no such element is already connected to these nodes,
(2) series augmentations of existing branches with series elements if no such element is already present.

Parallel augmentation of a given circuit described by its incidence matrix and types/values of branch elements is simply performed by adding an element connected to existing nodes. The new element is described by a new column appended in the incidence matrix, its type and value.

On the other hand, series augmentation is performed by adding an element in series to an existing branch. For this, the branch is split into two series-connected branches by adding a node appended to the list of existing nodes. The original branch is then reconnected between one of the original nodes and the new node, and the new branch is connected between the new node and the second original node. Consequently, the row size of the incidence matrix grows by one and some entries are modified to account for the reconnection. An additional column is appended to the incidence matrix to account for the new element.

To minimize user interaction, we propose to generate all possible series and parallel augmentations of a nominal circuit according to the two rules above. This operation can be performed once or several times, however, the complexity increases significantly after each step. The elements added by augmentation will account for parasitics, skin or proximity effects in high-frequency and will yield an automatically-generated broadband ECM.

4. ELEMENT PERTURBATION

We are provided with frequency responses of components obtained by direct measurement or using an electromagnetic field solver. Using minimal user insight, a nominal circuit is defined. This circuit is then augmented following Sect. 3. Lastly, we perturb the value of each circuit element to match the response of the new system to the given measurements.

4.1 Single element

We treat the case of a single element first and we distinguish between two scenarios based on its type:

- shunt element: (5) shows that the stamp of the element in the MNA system is recovered through the appropriate column of the incidence matrix. If the element is connected between nodes k and l, the selector vector ξ indicates its connectivity

$$
\xi = \begin{bmatrix} \mathbf{0} \\ 1 \\ \mathbf{0} \\ -1 \\ \mathbf{0} \end{bmatrix} \begin{array}{l} \\ \leftarrow \quad k^{th} \text{ entry} \\ \\ \leftarrow \quad l^{th} \text{ entry.} \\ \\ \end{array} \tag{9}
$$

If node k or l is the ground node, the corresponding row is deleted, hence ξ contains only 1 or -1.

- series element: (5) shows that the value of the element directly multiplies the corresponding current unknown in the state-space vector, hence

$$
\xi = \begin{bmatrix} \mathbf{0}_n \\ \mathbf{e}_L \\ \mathbf{0}_{n_r} \end{bmatrix} \text{ or } \xi = \begin{bmatrix} \mathbf{0}_n \\ \mathbf{0}_{n_l} \\ \mathbf{e}_R \end{bmatrix} \tag{10}
$$

for perturbing an inductance or a resistance, respectively. $\mathbf{0}_n$ is a null column vector of size n, the number of nodes, $\mathbf{0}_{n_r}$, of size n_r, the number of series resistive elements and $\mathbf{0}_{n_l}$, of size n_l, the number of series dynamic elements. Moreover, $\mathbf{e}_L$ is a unit column vector with 1 at the position of the corresponding inductor and similarly for $\mathbf{e}_R$.

Denoting $s\mathbf{E}_{dae} - \mathbf{A}_{dae}$ as $\mathcal{G}$, the transfer function is $\mathbf{H}(s) = \mathbf{C}\mathcal{G}^{-1}\mathbf{B}$ (note that $\mathcal{G}$ contains the frequency dependency). The perturbation induced in the element value induces a perturbation in $\mathcal{G}$ as follows:

$$
\mathcal{G} = \mathcal{G}_0 + \Delta\alpha\xi\xi^T, \tag{11}
$$

where $\mathcal{G}_0$ is the matrix containing the nominal values and $\Delta\alpha$ is the perturbation in the value of the element. If we treat a dynamic element, a capacitance or an inductance, then $\Delta\alpha = s\Delta C_i$ or $\Delta\alpha = s\Delta L_i$. For static elements, $\Delta\alpha = \Delta G_i$ or $\Delta\alpha = \Delta R_i$, respectively.

The Sherman-Morrison formula (Golub and Van Loan (1996)) allows to express $\mathcal{G}^{-1}$:

$$
\mathcal{G}^{-1} = \mathcal{G}_0^{-1} - \frac{\mathcal{G}_0^{-1}\Delta\alpha\xi\xi^T\mathcal{G}_0^{-1}}{1 + \Delta\alpha\xi^T\mathcal{G}_0^{-1}\xi}. \tag{12}
$$

Hence, the transfer function is

$$
\mathbf{H}(s) = \mathbf{C}\mathcal{G}^{-1}\mathbf{B} = \underbrace{\mathbf{C}\mathcal{G}_0^{-1}\mathbf{B}}_{\mathbf{H}_0(s)} - \Delta\alpha\frac{\overbrace{\mathbf{C}\mathcal{G}_0^{-1}\xi}^{\mathbf{F}_c(s)}\overbrace{\xi^T\mathcal{G}_0^{-1}\mathbf{B}}^{\mathbf{F}_b(s)}}{1 + \Delta\alpha\underbrace{\xi^T\mathcal{G}_0^{-1}\xi}_{K(s)}}
$$

$$
= \mathbf{H}_0(s) - \Delta\alpha\frac{\mathbf{F}(s)}{1 + \Delta\alpha \cdot K(s)}, \tag{13}
$$

with $\mathbf{F}(s) = \mathbf{F}_c(s)\mathbf{F}_b(s)$ (note that $K(s)$ is scalar).

We wish to minimize the deviation between the measurements provided, denoted by $\mathbf{H}_i$, and the transfer function of the perturbed system evaluated at the measurement frequencies ω_i, where $\omega_i = 2\pi f_i$, for $i = 1, \ldots, N$, with N, the number of samples provided: $\mathcal{E} = \sum_{i=1}^{N} \|\mathbf{H}(\mathrm{i}\omega_i) - \mathbf{H}_i\|_F^2$, so, after substitution of (13), the error becomes

$$
\mathcal{E} = \sum_{i=1}^{N} \left\| \left(\mathbf{H}_0(\mathrm{i}\omega_i) - \Delta\alpha\frac{\mathbf{F}(\mathrm{i}\omega_i)}{1 + \Delta\alpha \cdot K(\mathrm{i}\omega_i)} \right) - \mathbf{H}_i \right\|_F^2
$$

$$
= \sum_{i=1}^{N} \left\| \Delta\mathbf{H}(\mathrm{i}\omega_i) - \Delta\alpha\frac{\mathbf{F}(\mathrm{i}\omega_i)}{1 + \Delta\alpha \cdot K(\mathrm{i}\omega_i)} \right\|_F^2,
$$

with $\Delta\mathbf{H}_i = \mathbf{H}_0(\mathrm{i}\omega_i) - \mathbf{H}_i$. We redefine $\mathbf{F}(\mathrm{i}\omega_i)$ as $\mathbf{F}_i \in \mathbb{C}^{p \times p}$ and $K(\mathrm{i}\omega_i)$ as $K_i \in \mathbb{C}$, so the error expression becomes

$$
\mathcal{E} = \sum_{i=1}^{N} \left\| \Delta\mathbf{H}_i - \mathbf{F}_i\frac{\Delta\alpha}{1 + \Delta\alpha \cdot K_i} \right\|_F^2. \tag{14}
$$

The optimization problem is simply

$$
\min_{\Delta\alpha} \mathcal{E} = \min_{\Delta\alpha} \sum_{i=1}^{N} \left\| \Delta\mathbf{H}_i - \mathbf{F}_i\frac{\Delta\alpha}{1 + \Delta\alpha \cdot K_i} \right\|_F^2. \tag{15}
$$

The optimization parameter $\Delta\alpha$ appears in the numerator and denominator, making this problem nonlinear. Employing the Sanathanan-Koerner (SK) iteration (Sanathanan

and Koerner (1963)), we relax the problem by using $\Delta\alpha$ from the previous iteration in the denominator, thus yielding a linear problem which can be solved to determine the current $\Delta\alpha$:

$$\min_{\Delta\alpha} \sum_{i=1}^{N} \left\| \frac{\Delta\mathbf{H}_i + (\Delta\mathbf{H}_i K_i - \mathbf{F}_i)\,\Delta\alpha_k}{1 + \Delta\alpha_{k-1} \cdot K_i} \right\|_F^2 \quad (16)$$

via least-squares: $\mathbf{A}_{LS}\Delta\alpha_k \approx \mathbf{b}_{LS}$, with

$$\mathbf{A}_{LS} = \begin{bmatrix} \text{vec}(\Re(\mathbf{X}_1)) \\ \text{vec}(\Im(\mathbf{X}_1)) \\ \vdots \\ \text{vec}(\Re(\mathbf{X}_N)) \\ \text{vec}(\Im(\mathbf{X}_N)) \end{bmatrix}, \mathbf{b}_{LS} = \begin{bmatrix} \text{vec}(\Re(\mathbf{Y}_1)) \\ \text{vec}(\Im(\mathbf{Y}_1)) \\ \vdots \\ \text{vec}(\Re(\mathbf{Y}_N)) \\ \text{vec}(\Im(\mathbf{Y}_N)) \end{bmatrix}, \quad (17)$$

where vec is the vectorization of the $p \times p$ matrix in the argument, $\Re, \Im$ are the real and imaginary parts and lastly, $\mathbf{X}_i = \frac{\Delta\mathbf{H}_i K_i - \mathbf{F}_i}{1 + \Delta\alpha_{k-1} K_i}$ and $\mathbf{Y}_i = \frac{-\Delta\mathbf{H}_i}{1 + \Delta\alpha_{k-1} K_i}$.

4.2 Several elements

For perturbing several elements, we employ the alternating least squares technique. Each element is optimized independently by keeping the other parameters fixed and applying Sect. 4.1. This iterative process is run until convergence or a maximum number of iterations is reached. The pseudocode is detailed in Algorithm 1.

5. NUMERICAL EXAMPLES

5.1 RLC circuit with parasitic elements

The first example is a theoretical example (with unrealistic values) in which the goal is to identify the parasitic elements of an inductor and a capacitor in an RLC circuit. The circuit is shown in Fig. 2, with the parasitics indicated in red, the parasitic elements having values much smaller than those of the circuit elements. We model the inductor with value 1.5H as having an equivalent series resistance of .05Ω. Similarly, the capacitor with value .22F is modeled together with a series resistance of .005Ω and a series inductance of .03H.
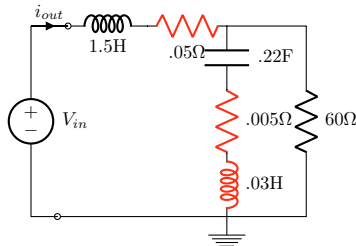

Fig. 2. RLC circuit with parasitics

We consider admittance parameters for the circuit in Fig. 2, by having the circuit voltage-controlled and measuring the current in the first branch. We generate 200 measurements of the admittance parameters for this circuit between $\omega = 1$ and $\omega = 10$rad/s. We start from the RLC circuit with no parasitic elements, which we augment using all possible series augmentations by R and L elements and parallel augmentations by G and C elements. Afterwards, topological fitting is applied to the augmented circuit by perturbing the values of the augmented elements and the values found are indicated next to each element in Fig. 3

Algorithm 1: top_fit

Input : $(f_i, \mathbf{H}_i), \forall i = 1, \ldots, N$: measurements,
$\mathbf{R}_0$: diagonal matrix with input impedance at each port: ∞ (impedance), 0 (admittance), real positive (scattering),
$\mathbf{A}$: reduced incidence matrix,
nodes: structure with node information,
list_el: list of elements as a cell array of strings {'R','L','C','G'},
val_el: vector of nominal values,
ind_el: vector of indices for the elements to be perturbed
opts: structure with tolerance and maximum iterations number

Output: new_val_el: vector of new numerical values
$\mathbf{E}_{dae}, \mathbf{A}_{dae}$: updated descriptor-form

1 $[\mathbf{A}_C, \mathbf{A}_G, \mathbf{A}_L, \mathbf{A}_R, \mathbf{C}_b, \mathbf{G}_b, \mathbf{L}_b, \mathbf{R}_b, i_C, i_G, i_R, i_L] =$ get_top($\mathbf{A}$,list_el,val_el) // Obtain circuit topology as in (3) and (4)
2 nx = #rows($\mathbf{A}$)+size($\mathbf{L}_b$)+size($\mathbf{R}_b$)
3 $[\mathbf{A}_R, \mathbf{R}_b, \mathbf{B}, \mathbf{C}]$ = add_top_ports(nx,nodes,$\mathbf{R}_0,\mathbf{A}_R,\mathbf{R}_b$) // Based on Z-/Y-/S-formulation, extend $\mathbf{A}_R$ and $\mathbf{R}$ as needed and create $\mathbf{B}$ and $\mathbf{C}$
4 $[\mathbf{E}_{dae}, \mathbf{A}_{dae}]$ = construct_DAE($\mathbf{A}_C, \mathbf{A}_G, \mathbf{A}_L, \mathbf{A}_R, \mathbf{C}_b, \mathbf{L}_b$,
5 $\mathbf{G}_b, \mathbf{R}_b$) // Constructs A and E as in (5)
6 ξ = create_xi(ind_el,list_el,$i_C, i_G, i_L, i_R, \mathbf{A}_C, \mathbf{A}_G, \mathbf{A}_L, \mathbf{A}_R$, size($\mathbf{E}_{dae}$))// selector vectors as in (9),(10)
7 nIter$_1$ = 0, $\epsilon_1 = \infty$// outer loop
8 $\overline{\alpha} = \mathbf{0}$ // initial guess
9 $\Delta\alpha = \mathbf{0}$// stores increments
10 $\widetilde{\alpha}$ =val_el(ind_el)// stores current values
11 **while** *nIter$_1$ <opts.maxIter & ϵ_1 >opts.tol* **do**
12   **for** *j* **do**
13     $\xi = \xi_j$
14   **for** *i* **do**
15       $\lfloor$ Compute $\Delta\mathbf{H}_i$, $\mathbf{F}_i$ and K_i
16     $\alpha = \overline{\alpha}_j$, nIter$_2$ = 0, $\epsilon_2 = \infty$// inner loop
17   **while** *nIter$_2$ <opts.maxIt & ϵ_2 >opts.tol* **do**
18   nIter$_2 \leftarrow$ nIter$_2$ + 1
19   Form $\mathbf{A}_{LS}$ and $\mathbf{b}_{LS}$ as in (17)
20   Solve $x = \mathbf{A}_{LS}\backslash\mathbf{b}_{LS}$ imposing $x + \widetilde{\alpha}_j > 0$
21       $\lfloor$ $\epsilon_2 \leftarrow |\alpha - x|$, $\alpha \leftarrow x$
22     $\Delta\alpha_j \leftarrow \alpha$, $\widetilde{\alpha}_j \leftarrow \widetilde{\alpha}_j + \alpha$
23   Update $\mathbf{C}_b, \mathbf{L}_b, \mathbf{G}_b$ or $\mathbf{R}_b$ with new value $\widetilde{\alpha}_j$ and $\mathbf{E}_{dae}, \mathbf{A}_{dae}$ with construct_DAE
24   nIter$_1 \leftarrow$ nIter$_1$ + 1, $\epsilon_1 \leftarrow \|\Delta\alpha\|_2$
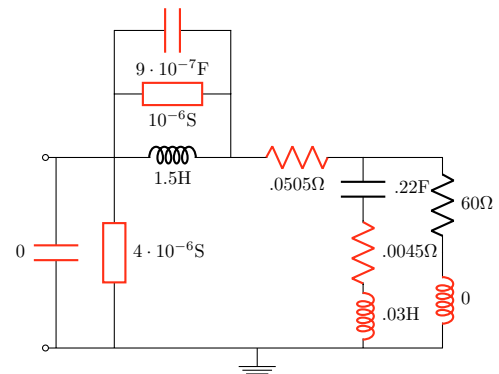25 new_val_el = val_el, new_val_el(ind_el) = $\widetilde{\alpha}$

Fig. 3. Augmented RLC circuit with the values found

(the conductance is represented as a rectangle, while the resistor is displayed using the zig-zag symbol).

Lastly, Fig. 4 shows the Y-parameter measurements of the circuit in Fig. 2, which, together with the RLC circuit with no parasitics, are used as input parameters to our approach to recover the circuit in Fig. 3.
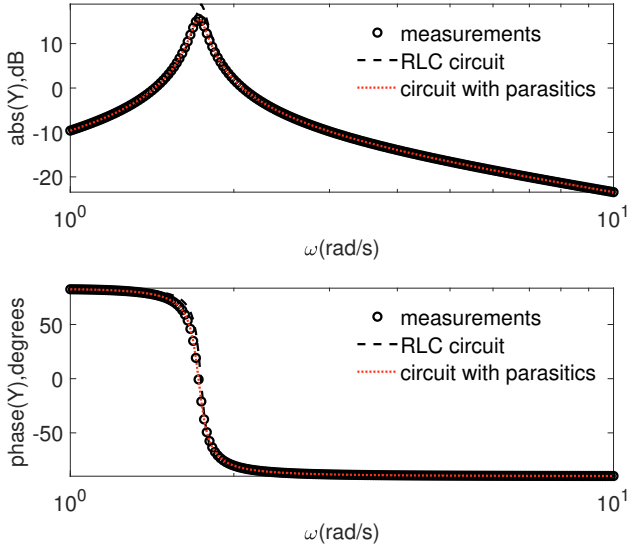

Fig. 4. Results for the RLC circuit with parasitics

Comparable results were obtained when adding white Gaussian noise with 60dB signal-to-noise ratio to the measurements. The circuit found is shown in Fig. 5 while results are similar to those in Fig. 4. The noise level was chosen such that the parasitic elements with values in the 10^{-3} range are not embedded in noise.
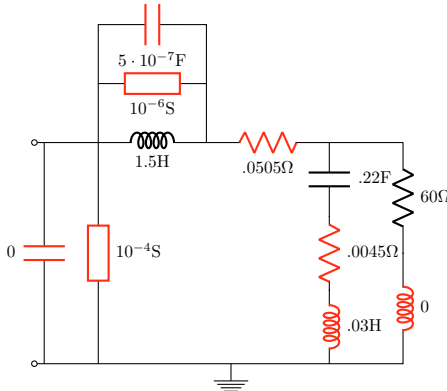

Fig. 5. RLC circuit with augmented elements and their values found in the presence of noise

5.2 Spiral inductor

S-parameter measurements obtained from a full-wave electromagnetic field simulation of a 2-port spiral inductor are provided.

We normalize the frequency by $\omega_{\mathrm{norm}} = 10^{-10} \mathrm{rad/s}$. Inductances and capacitances are rescaled by the same factors $L_{\mathrm{norm}} = 10^{-10}$ H and $C_{\mathrm{norm}} = 10^{-10}$ F, while impedances are normalized by a unit factor $R_{\mathrm{norm}} = 1\,\Omega$. Reported component values are normalized quantities with no units and actual values are found as

$$L = L_{\mathrm{norm}}\hat{L}, \quad C = C_{\mathrm{norm}}\hat{C}, \quad R = R_{\mathrm{norm}}\hat{R}.$$

We first fit a π configuration (Fig. 6) to the first half of the frequency band to find the elements matching this low-frequency behaviour. The initial guesses for the elements' values are 10^{-7} (this is the nominal circuit for this step). The values found with `top_fit` yield a model which matches accurately the first half of the measurements (shown in Fig. 7).
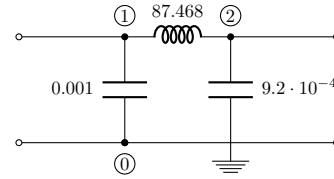

Fig. 6. π-configuration found from the low-frequency behavior of the spiral inductor (normalized component values)
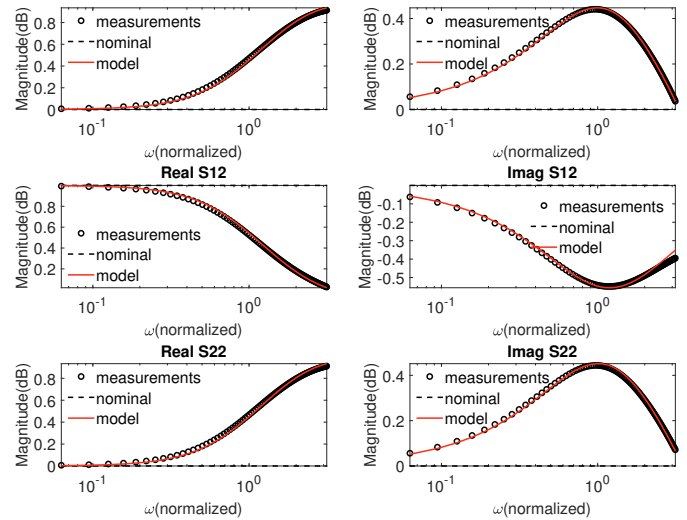

Fig. 7. Fitting the π configuration in low-frequency

In the next step, we duplicate this circuit to obtain a 2π configuration, thus accounting for proximity effects (Cao et al. (2003); Wang et al. (2006)). We distribute the inductor value found in the first step and use the value found in Fig. 6 divided by two as initial guess for the two inductors, while the initial guess for the last capacitor is 10^{-7}. This constitutes the nominal circuit for this step. Topological fitting is applied again on the whole frequency band. The circuit found is depicted in Fig. 8. The measurements, the response of the nominal model and the response corresponding to the circuit in Fig. 8 are shown in Fig. 9. This circuit fits the measurements quite accurately, with a slight discrepancy still observed in the imaginary part of S_{12}.
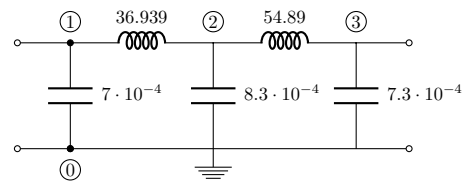

Fig. 8. 2π-configuration for the spiral inductor (normalized component values)

In the last step, we generate all possible series and parallel augmentations of the 2π circuit of Fig. 8 (this is the
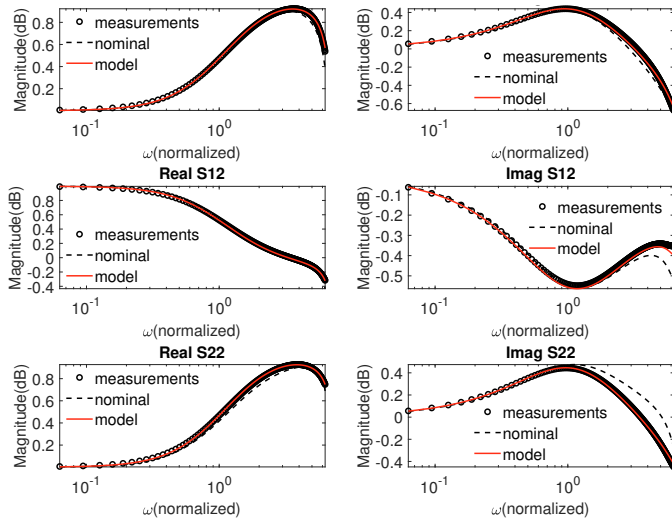
Fig. 9. Fitting the 2π configuration on the entire frequency band

nominal circuit for the last step) and perform topological fitting to find the missing parasitic elements which would improve the accuracy in high-frequency. The resulting circuit is displayed in Fig. 10; it matches the data closely over the entire frequency band, as shown in Fig. 11.
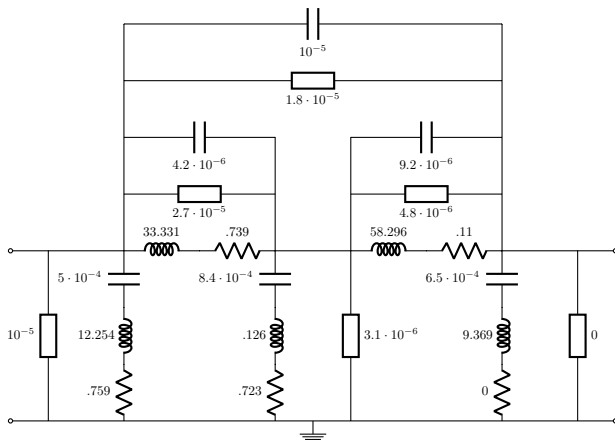

Fig. 10. Circuit obtained after applying topological fitting on the circuit obtained by all possible series and parallel augmentations of the 2π configuration (normalized component values)

6. CONCLUSION

This paper aims to make a step towards automated generation of equivalent circuit models for components. These models are valid in a broad-band and are stable and passive by construction. The algorithm works well for simple topologies with few circuit elements, but may run into difficulties if the size grows too large or if the topology of the nominal circuit is not suitable for the application at hand. In the future, we consider combining the SK process with a Newton iteration and use regularization for alternate least-squares to improve and speed up convergence.

REFERENCES

Cao, Y., Groves, R.A., Huang, X., Zamdmer, N.D., Plouchart, J.O., Wachnik, R.A., King, T.J., and Hu, C.
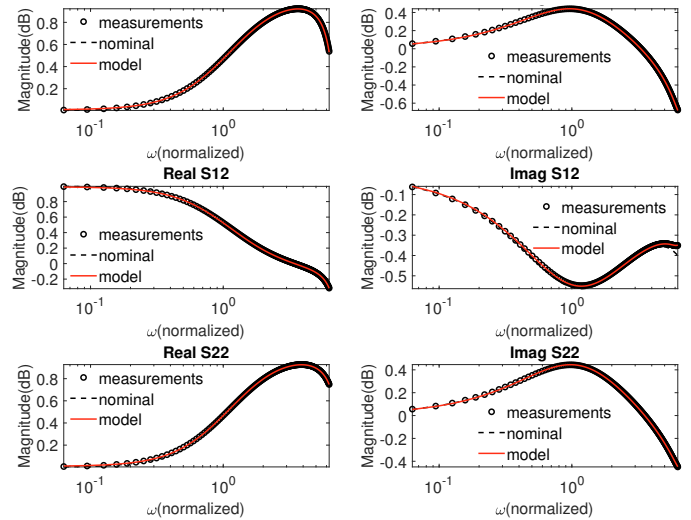

Fig. 11. Fitting the augmented circuit on the entire frequency band

(2003). Frequency-independent equivalent-circuit model for on-chip spiral inductors. *IEEE Journal of Solid-State Circuits*, 38(3), 419–426.

Golub, G.H. and Van Loan, C.F. (1996). *Matrix computations*, volume 3. Johns Hopkins Univ Pr.

Grivet-Talocia, S. and Gustavsen, B. (2015). *Passive Macromodeling: Theory and Applications*. John Wiley and Sons, New York.

Ho, C.W., Ruehli, A., and Brennan, P. (1975). The modified nodal approach to network analysis. *IEEE Trans. on Circuits and Systems*, 22(6), 504–509.

Kolstad, J., Blevins, C., Dunn, J.M., and Weisshaar, A. (2006). A new circuit augmentation method for modeling of interconnects and passive components. *IEEE Transactions on Advanced Packaging*, 29(1), 67–77.

Li, Y. and Wei, Z. (2015). A high-frequency scalable model for thin-film resistor on gan substrate. In *International Conference on Communication Technology (ICCT)*, 589–592.

Paul, D., Nakhla, M.S., Achar, R., and Weisshaar, A. (2009). Broadband modeling of high-frequency microwave devices. *IEEE Transactions on Microwave Theory and Techniques*, 57(2), 361–373.

Sanathanan, C. and Koerner, J. (1963). Transfer function synthesis as a ratio of two complex polynomials. *IEEE Trans. on Automatic Control*, 8(1), 56–58.

Sullivan, C.R., Sun, Y., and Kern, A.M. (2002). Improved distributed model for capacitors in high-performance packages. In *2002 IEEE Industry Applications Conference*, volume 2, 969–976.

Vlach, J. and Singhal, K. (1983). *Computer methods for circuit analysis and design*. Springer.

Wang, X., Ren, J., Yang, F., Zheng, W., Yu, Q., Ning, N., and Yang, M. (2006). A wide-band 2π equivalent-circuit model for spiral inductors on silicon. In *International Conference on Communications, Circuits and Systems*, volume 4, 2605–2609.

Zhaoqing, L. (2015). *SPICE Compatible Macromodels of Linear Multiport Networks*. Master's thesis, McGill University, Montreal, Canada.